Applied Catalysis B: Environmental 115–116 (2012) 236–244

Contents lists available at SciVerse ScienceDirect

Applied Catalysis B: Environmental

journal homepage: www.elsevier.com/locate/apcatb

Ethanol supercritical route for fabricating bimodal carbon modified mesoporous TiO_2 with enhanced photocatalytic capability in degrading phenol

Ya Zhang, Peng Zhang, Yuning Huo, Dieqing Zhang, Guisheng Li*, Hexing Li

Key Laboratory of Resource Chemistry of Ministry of Education, Shanghai Key Laboratory of Rare Earth Functional Materials, College of Life and Environmental Science, Shanghai Normal University, Shanghai 200234, PR China

ARTICLE INFO

Article history:
Received 1 November 2011
Received in revised form
16 December 2011
Accepted 19 December 2011
Available online 28 December 2011

Keywords:
Bimodal carbon-modification
TiO_2
Supercritical
Phenol
Photocatalytic

ABSTRACT

This paper reports the fabrication of a novel mesoporous C-TiO_2 photocatalyst via an ethanol supercritical solvothermal method involving tetrabutyl titanate and raw rice. Such as-prepared C-TiO_2 possessed a bimodal carbon-modification effect, including carbon doping in the lattice of TiO_2 and carbon sensitizing the surface of TiO_2. The ethanol supercritical treatment also contributed mesoporous structure with large surface area (160 m^2/g) and high crystallinity of anatase to the C-TiO_2. These materials exhibited an excellent photocatalytic performance and recyclability for phenol oxidation under visible light irradiation ($\lambda > 420$ nm). The C-TiO_2 samples were characterized by using X-ray diffraction (XRD), Brunauer–Emmett–Teller (BET), transmission electron microscopy (TEM), X-ray photoelectron spectroscopy (XPS), temperature-programmed oxidation (TPO), Raman and ultraviolet–visible reflectance (UV–vis) spectroscopy. The relationship between the physicochemical property and the photocatalytic performance of the as prepared samples is discussed. We also investigate the effect of the supercritical temperature and calcining temperature on the photocatalytic performance of the obtained C-TiO_2. The present work explores an effective supercritical fluid based route for the fabrication of mesoporous C-TiO_2 with bimodal carbon modification effect and high photocatalytic performance for treating phenol, which can be extended to synthesize other functional photocatalytic materials.

1. Introduction

Photocatalysis, as a novel technique, has attracted increasing attentions due to its potential applications in solar energy conversion as well as solving environmental problems. Owing to its non-toxicity, abundance, high photostability and high efficiency [1,2], titanium dioxide (TiO_2) has been widely used in organic pollutants mineralization, water splitting, and CO_2 fixation [3–5]. However, its wide band gap ($E_g = 3.2$ eV) only allows TiO_2 to be excited by UV light (accounting for merely 4–5% sun light spectrum on the earth surface). Thus, extending the band edge of TiO_2 to long wavelength light is still a great challenge task for photocatalytic research. Doping TiO_2 with various species has been proved as an effective route for enhancing the photocatalytic performance in visible light region, attributed either to introduction of intragap localized states by the dopants [6–8] or to narrowing of the band gap [9–11]. Transition metal ions were introduced into the framework of TiO_2 to extend the band edge via various routes [12–14], nevertheless, the visible-light induced photocatalytic efficiency of these metal doped TiO_2 is still very low because of the atom diffusion and the increased hole–electron recombination of defect sites [15].

Compared to metal doping, non-metal doping of TiO_2 has been proved much more effective. Up to date, many works concerning TiO_2 doped by C, N, or S have been reported, and these materials display a remarkable improvement in visible-light photocatalytic efficiency [16–18]. Among the various non-metal elements, carbon doping has attracted significant attentions. Different synthetic methods have been explored to incorporate carbon into the lattice of TiO_2. Carbon-doped TiO_2 for photocatalytic hydrogen production has been reported by Khan et al. [16]. This material was prepared via the direct combustion of metallic titanium sheets in a natural gas flame at 850 °C. Irie et al. further reported the fabrication of carbon-doped anatase TiO_2 powders via oxidative annealing of TiC under O_2 flow at 600 °C [19]. It has to be recognized that high temperature calcination treatment is always required to incorporate carbon species into the lattice of TiO_2, resulting in the serious aggregation of TiO_2 crystals with low surface area and pore volume. Fortunately, ethanol supercritical fluid has been proved as a mild route for incorporating hybrid atoms (S and N) in the lattice of TiO_2 at low temperature, producing porous structures, high surface area, and high crystallization degree of anatase TiO_2 owing to the extremely low surface intension of supercritical fluid [18,20–22]. Except for being served as dopants, carbon species were utilized

* Corresponding author. Tel.: +86 21 64322272; fax: +86 21 64322272.
E-mail address: Liguisheng@shnu.edu.cn (G. Li).

0926-3373/$ – see front matter © 2011 Elsevier B.V. All rights reserved.
doi:10.1016/j.apcatb.2011.12.031

as surface sensitizer to improve the visible-light induced photocatalytic activity of TiO_2 [23,24]. The nanosized carbon on the TiO_2 surface can take up the photo-excited electrons to accelerate the separation of photoelectrons and holes, producing a structure sensitizing TiO_2 for absorbing more light. Such new insights explored a novel route for fabricating novel TiO_2/C composite photocatalysts. Thus, it is highly required to modify TiO_2 with carbon serving as both dopants in the TiO_2-lattice and sensitizer on the TiO_2-surface. Such synergistic bimodal modification effect of carbon may play an important role for enhancing the photocatalytic performance of TiO_2 in visible light region. However, it is very difficult to realize the bimodal modification of TiO_2 with carbon at one-pot synthesis, because doping carbon into the TiO_2-lattice always needs high temperature calcinations and sensitizing TiO_2 with carbon should be performed under moderate conditions, such as solvothermal treatment.

Herein, we proposed a solvothermal route in ethanol supercritical fluid to synthesize C@TiO_2 with bimodal modification effect by using tetrabutyl titanate and raw rice as titanium and carbon resources, respectively. Such ethanol supercritical condition not only allowed bimodal carbon modification, but also produced mesoporous structure with large surface area and high crystallinity of anatase TiO_2. Owing to the synergetic effect of doping and sensitizing of carbon, large surface area, and high crystallinity, the as-obtained C-TiO_2 exhibited an excellent activity during the photocatalytic degradation of phenol under visible light irradiation. Importantly, these mesoporous C-TiO_2 catalysts showed excellent stability and maintained a high level of photocatalytic activity after multiple reaction cycles.

2. Experimental

2.1. Preparation of C-TiO_2

All chemicals were analytical grade and used as received without further purification. In a typical procedure, 1.0 g raw rice was added into a uniform solution containing 5 mL of tetrabutyl titanate (TBOT) and 25 mL of absolute ethanol solution under vigorous stirring for 15 min at room temperature. The mixed precursor solution was transferred into an autoclave (500 mL) containing 170 mL of absolute ethanol solution. The autoclave was further heated slowly to 250, 260, and 270 °C with a heating rate of 4 °C/min. Upon keeping the ethanol supercritical conditions for 3 h, the supercritical system was cooled slowly to room temperature naturally. Then, the residual rice was separated from the resulted suspension. Finally, the as-obtained precipitate was centrifugated and washed with distilled water and ethanol for four times, and dried in vacuum at 80 °C overnight. The carbon modified TiO_2 sample prepared at 260 °C under supercritical conditions was denoted as C-TiO_2-260. The as-prepared C-TiO_2-260 sample calcined at 300 °C was denoted as C-TiO_2-260-300. For comparison, pure TiO_2 was also prepared in the absence of raw rice without changing the other conditions, denoted as TiO_2-260.

2.2. Characterization of photocatalysts

X-ray diffraction (XRD) patterns were collected on Rigacu Dmax-3C (Cu Kα radiation). The crystal size was estimated from the Scherrer equation, $D = K\lambda/(\beta\cos\theta)$, where D is the crystal size, K is the wavelength of the X-ray radiation (0.1541 nm) and usually taken as 0.89, β is the peak widths at half-maximum height of the sample. Transmission electronic micrograph (TEM) and selected area electronic diffraction (SAED) were recorded on a JEM-2010. The N_2 sorption isotherms were obtained on a NOVA 4000 at −196 °C, from which the surface area (S_{BET}), pore volume (V_P), and average pore diameter (d_P) were calculated by using BJH method. Raman spectra were recorded on Raman spectrometer (Dilor Super LabRam II). UV–vis diffuse reflectance spectra (DRS) were obtained using a scan UV/vis spectrophotometer (DRS, MC-2530) equipped with an integrating sphere assembly, while $BaSO_4$ was used as a reference. Photoluminescence (PL) emission spectra were measured on Varian Cary-Eclipse 500 at room temperature under the excitation light at 358.5 nm. The X-ray photoelectron spectroscopy (XPS) analysis was performed on a Perkin-Elmer PHI 5000C. All the binding energies were calibrated by using the contaminant carbon (C_{1s} = 284.6 eV) as a reference. FT-IR spectra on pellets of the samples mixed with KBr were recorded on a Nicolet Magna 560 FT-IR spectrometer at a resolution of 4 cm^{-1}. Temperature programmed oxidation (TPO) measurements were carried out on the apparatus micrometritics II 2920. About 100 mg of the as-obtained catalyst was degassed at 200 °C under He for 2 h. After cooling down to 40 °C in the blanket of He, the gas was switched to 5 vol.% O_2/He (50 mL/min), and the sample was heated to 800 °C at a ramping rate of 10 °C/min. The amount of O_2 consumed was monitored by thermal conductivity detector.

2.3. Photoelectrochemical properties testing

Photoelectrochemical measurements were carried out in a conventional three-electrode, single-compartment quartz cell on an electrochemical station (CHI 660D). The Ti/C@TiO_2 electrode and Ti/TiO_2 electrode with an active area of ca. 2 cm^2 were served as working electrode. The counter electrode and the reference electrode were platinum sheet and saturated calomel electrode (SCE), respectively. A 300 W Xe lamp with an ultraviolet filter (λ > 420 nm and λ > 550 nm) was used as visible light source and positioned 10 cm away from the photoelectrochemical cell. A 0.2 M Na_2SO_4 aqueous solution was used as the electrolyte. Ti/C@TiO_2 and Ti/TiO_2 electrodes were prepared as follows: 0.2 g of C@TiO_2 and TiO_2 were added in ethanol (20 mL) and sonicated for 1 h, then Ti substrates (3.3 cm × 2 cm) were dipped into the complex precursor for 3 min and then were pulled out with a velocity of 3 cm min^{-1}. Then the sample was dried at 100 °C for 12 h.

2.4. Activity testing

The liquid-phase photocatalytic degradation of organic pollutants phenol and methyl orange are carried out at 303 K in an 80 mL self-designed quartz photochemical reactor containing 0.050 g photocatalyst and 50 mL 0.020 g L^{-1} pollutant aqueous solution. After being vigorously stirred for 1 h which is long enough for the reactant to reach adsorption–desorption equilibrium on the catalyst. The photocatalytic reaction was initiated by irradiating the system with 300 W xenon lamp located at 30 cm away from the reaction solution. All the UV lights with wavelength less than 420 nm were removed by a Pyrex glass filter. The degradation rate of phenol was analyzed by a UV spectrophotometer (UV 7504/PC) at its characteristic wavelength (λ_{phenol} = 270 nm). Preliminary tests demonstrate a good linear relationship between the light absorbance and the pollutants concentration. Only less than 2% pollutants decomposed after reaction for 2 h under the same condition in the absence of either the catalyst or the light irradiation and, thus, could be neglected in comparison with the phenol degraded via photocatalysis. The reproducibility is checked by repeating the results at least 3 three times, and was found to be within acceptable limits (±5%). Hydroxyl radicals (•OH) trapping experiment was performed as follows: C-TiO_2 samples were evaluated at 30 °C in a beaker with aqueous suspensions of in 0.05 M terephthalic acid (TA) and 0.10 M NaOH solution (50 mL) containing 50 mg of catalyst powder. The suspensions were stirred for 30 min in the dark. At given time intervals with visible light

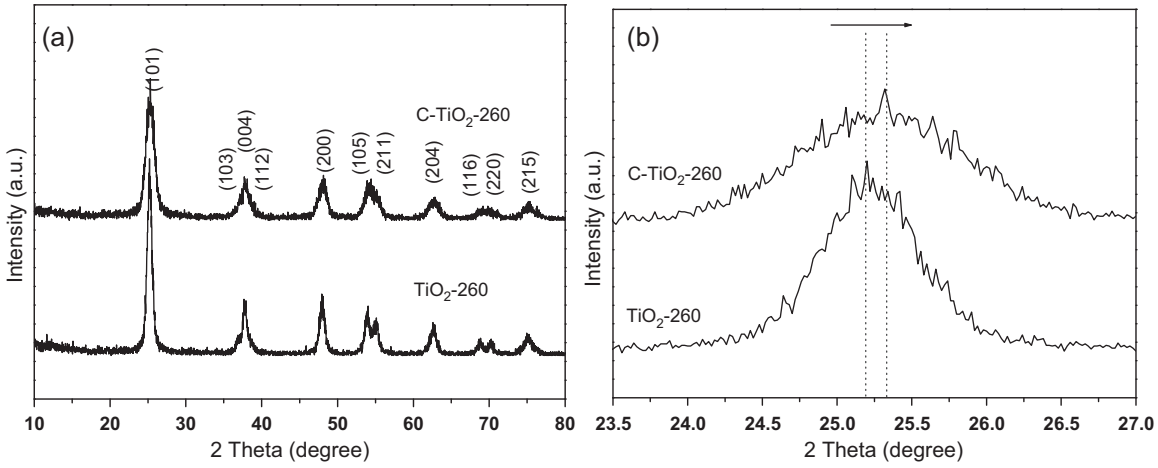

Fig. 1. (a) XRD patterns of TiO_2-260 and C-TiO_2-260 samples. (b) Shift of XRD patterns.

($\lambda > 420$ nm) irradiation, ca. 3 mL suspension was got into plastic tube and centrifuged to remove the photocatalyst particles. The photoluminescence intensity of TAOH was surveyed by a PLS Varian Cary-Eclipse 500 spectrophotometer.

3. Results and discussion

3.1. Composites characterization

Fig. 1a shows the typical X-ray diffraction (XRD) patterns of the as-prepared carbon-modified TiO_2 (C-TiO_2-260) and pure TiO_2 (TiO_2-260) samples. The intense and sharp diffraction peaks in this pattern suggest that the as-synthesized products are well-crystallized and could be consistent with anatase TiO_2 (JCPDS No. 21-1272). Furthermore, no diffraction peaks of the other impurities, such as graphite carbon, were observed. It should be also noted that the crystal size of sample C-TiO_2-260 is about 6.1 nm (calculated based on XRD results) using a Scherrer equation, much smaller than that (11.0 nm) of sample TiO_2-260. Such greatly decrease of the crystal size is attributed to the modification of carbon, which can effectively inhibit the further aggregation of the TiO_2 anatase crystals. Such conclusion can also be supported by the lattice distortion effect of anatase TiO_2. Compared to TiO_2-260, a slight shift to higher angles for the (1 0 1) diffraction peak of C-TiO_2-260 sample was observed in Fig. 1b. It is reasonable that such slight shift resulted from the lattice distortion of anatase TiO_2 caused by the incorporation of carbon into the lattice of TiO_2 owing to the difference in atomic radius of oxygen and carbon [25]. Nevertheless, the distortion did not affect the formation of anatase phase.

The transmission electron microscopy (TEM) images in Fig. 2a show clearly that C-TiO_2-260 sample is composed of numerous ultra-fine nanoparticles. These nanoparticles were closely aggregated each other to form a wormlike mesoporous structure. The selected-area electron diffraction (SAED) pattern of C-TiO_2-260 sample was also recorded (inset of Fig. 2a). The diffraction fingers ascribed to [1 0 1], [1 0 3] and [2 0 0] planes of anatase TiO_2 can be clearly defined, indicating the formation of good anatase crystallinity. The high resolution TEM (HRTEM) images in Fig. 2b further demonstrates that such mesoporous carbon doped TiO_2 sample was made of anatase TiO_2 nanocrystals (ellipses). The particle size of C-TiO_2-260 sample was estimated to 5–6 nm. This result was in good agreement with the evaluation obtained using a Scherrer equation based on the XRD patterns. Such high anatase crystallinity of the mesoporous carbon doped TiO_2 is highly desirable in photocatalysis [26]. In the absence of carbon modification, the crystal size of TiO_2-260 sample was increased to about 12 nm, as shown in the TEM images of Fig. 2c and d. The nitrogen adsorption-desorption isotherms and pore size distribution plots for TiO_2-260 and C-TiO_2-260 samples are illustrated in Fig. 2e and f. Both samples exhibit a type-IV isotherm being representative of mesoporous solids according to IUPAC classification [27]. The specific surface area of C-TiO_2-260 sample is 160 m^2/g calculated by the Brunauer–Emmett–Teller (BET) method. The pore diameter of C-TiO_2-260 is 1.8 nm (estimated using the desorption branch of the isotherm) with very narrow pore size distribution. The pure TiO_2 sample possesses virtually identical average pore diameter (2.5 nm) and specific surface area (138 m^2/g). It is clear that the ethanol supercritical conditions may allow the obtained sample to possess mesoporous structure in the absence of surfactants or other structure directing agents. Meanwhile, the modification of carbon can contribute a 16% increase of surface area to pure TiO_2, indicating that doping carbon can effectively prohibit the aggregation of nanoparticles. This is consistent with the conclusion of the XRD patterns. Such mesoporous architecture with large surface area plays an important role in catalyst design for its being able to improve the molecular transport of reactants and products [28].

In order to analyze the chemical and bonding environment of the TiO_2 matrix and carbon phase, X-ray photoelectron spectroscopy (XPS) investigation was conducted as shown in Fig. 3a–c. The binding energy of Ti $2p_{3/2}$ and O 1s are 458.4 eV and 529.7 eV, respectively, which is virtually identical to those for standard anataseTiO_2. Curve fitting analysis of C 1s high-resolution XPS spectra, as shown in Fig. 3c, affords four peaks at 284.9, 285.8, 288.2 and 288.6 eV for C-TiO_2-260. Among which, a part of C atoms (as observed at 284.9 eV) could be ascribed to adventitious elemental carbon (sp^2 hybridized carbon (BE = 284.6 eV)) [24]. The peaks at 285.8 and 288.6 eV are assigned to the oxygen bound species C—O and C═O respectively [29]. The peak at 288.2 eV is ascribed to the carbon incorporated into the TiO_2 lattice [30]. These results strongly suggest that partial carbon atoms were incorporated into the TiO_2 lattice and some of hybridized carbonate species were grafted on the surface of TiO_2 crystals under the ethanol supercritical conditions. Both the two carbon modification models could lead to the narrowing of the band-gap in obtained carbon-modified TiO_2. The Raman spectra of as made materials further confirmed the formation of carbon modified anatase indirectly. As shown in Fig. 3d, the peaks of pure TiO_2 around 145.5 cm^{-1} (E_g), 199 cm^{-1} (E_g, weak), 399 cm^{-1} (B 1g), 516 cm^{-1} (A 1g), and 640 cm^{-1} (E_g) can be ascribed to the characteristic peaks of the anatase phase [31], which are consistent with XRD results. The main peak around 148 cm^{-1} (148.2 cm^{-1}) in C-TiO_2-260 shows a slight shift to higher wave numbers compared with the pure TiO_2, which could be attributed

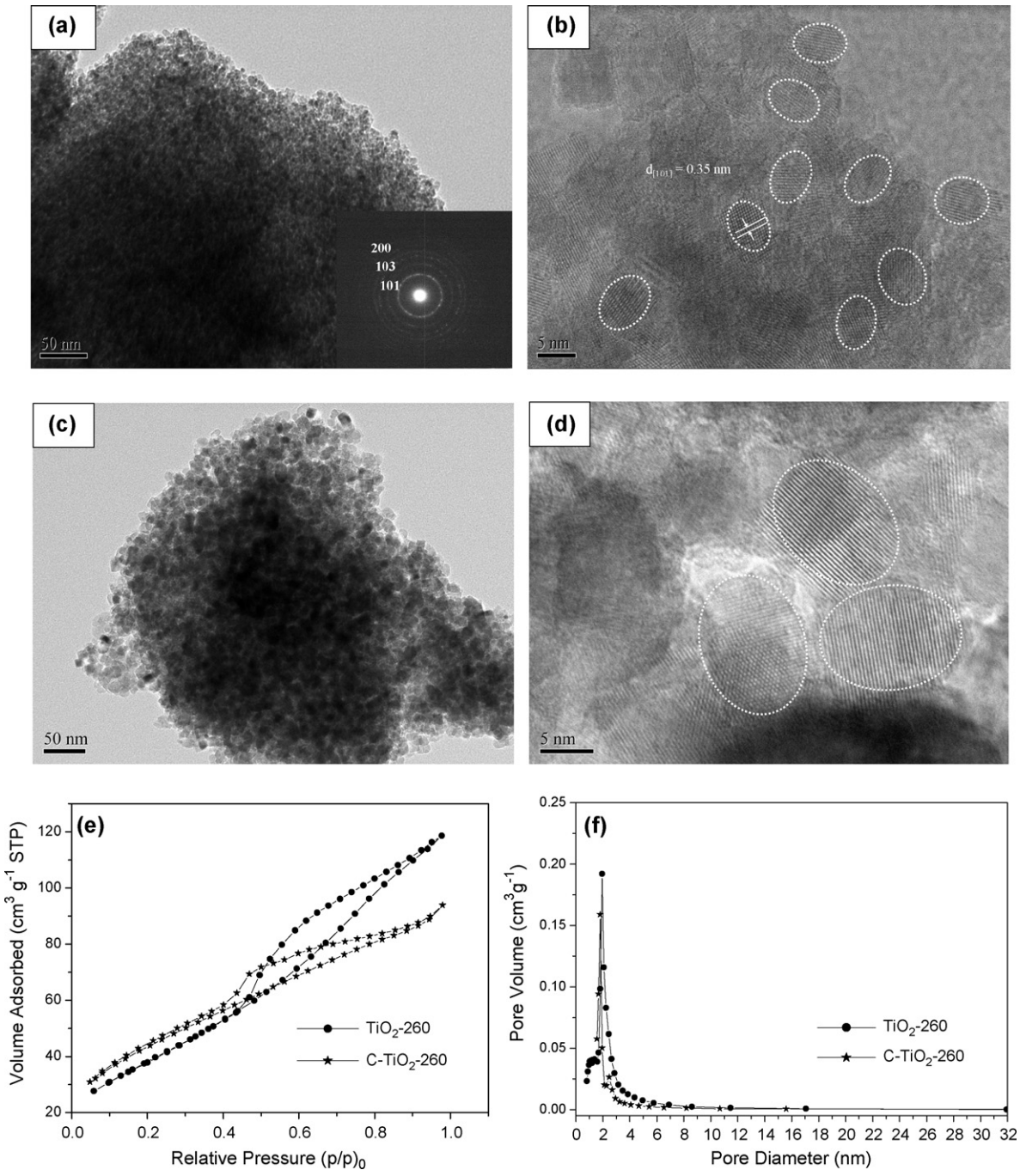

Fig. 2. TEM (a) and HRTEM (b) of C-TiO_2-260, TEM (c) and HRTEM (d) of TiO_2-260, N_2-sorption isotherms (e) and corresponding pore-size distribution curves (f) of TiO_2-260 and C-TiO_2-260.

to the oxygen vacancies and/or defects [32] induced by the carbon doping in the lattice and the hybridization on the surface of TiO_2. It should be noted that the titania relaxation intensity of the carbon modified sample (C-TiO_2-260) is much lower than that of the pure TiO_2 sample (TiO_2-260), probably due to a significant majority of light being absorbed and partly transformed into separated charges within the carbon-TiO_2 hybrid material [24].

The bonding characteristics of functional groups of TiO_2-260 and C-TiO_2-260 samples were identified by FT-IR spectroscopy, as shown in Fig. 4a. The absorption peaks at about 3400 and 1630 cm^{-1} are associated with the stretching vibrations of the hydroxyl groups and molecular water on the two samples [33]. To the case of C-TiO_2-260, the peak at 1046 cm^{-1} is due to the C—O stretches, and the peaks at 1447 and 1379 cm^{-1} are attributed to the C=O stretches [34]. However, no peaks related to —CH, —CH_2, or —CH_3 bonds can be observed, suggesting that no organic species exist on the surface of C-TiO_2. Temperature programmed oxidation (TPO) of C-TiO_2-260 sample was also performed to investigate the characteristics of carbon in C-TiO_2-260. As shown in Fig. 4b, the first oxygen consumption peak at 300 °C is attributed to the inflammation of residual carbon species on the nanoparticles surfaces. The oxygen consumption peak at 350 °C results from the thermal oxidation of elemental carbon on the surface of TiO_2 [25]. The third oxygen consumption peak at 450 °C is ascribed to the thermal oxidation of doped carbon in the lattice of TiO_2. No apparent peak can be observed over 500 °C, indicating that nearly all the carbon

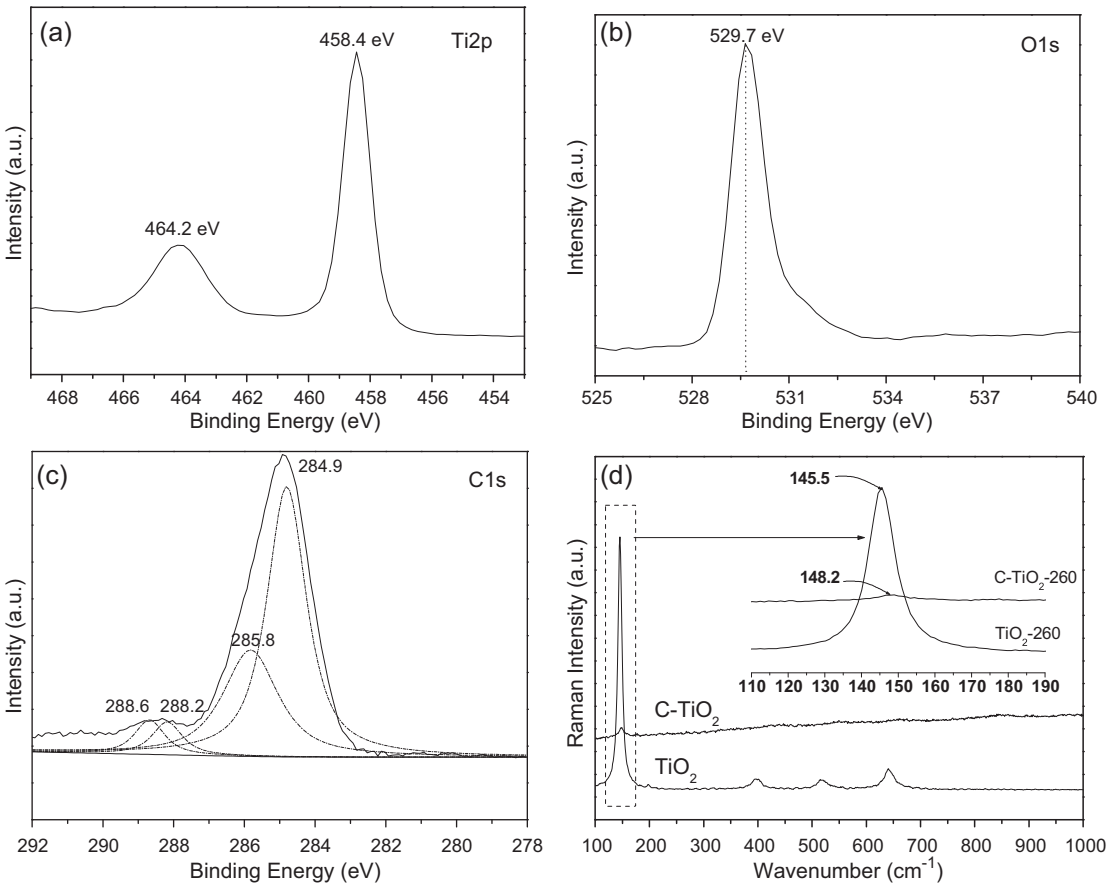

Fig. 3. XPS spectra of C-TiO_2-260: (a) Ti 2p, (b) O 1s and (c) C 1s of C-TiO_2-260 sample and Raman spectra (d) of the samples both TiO_2-260 and C-TiO_2-260.

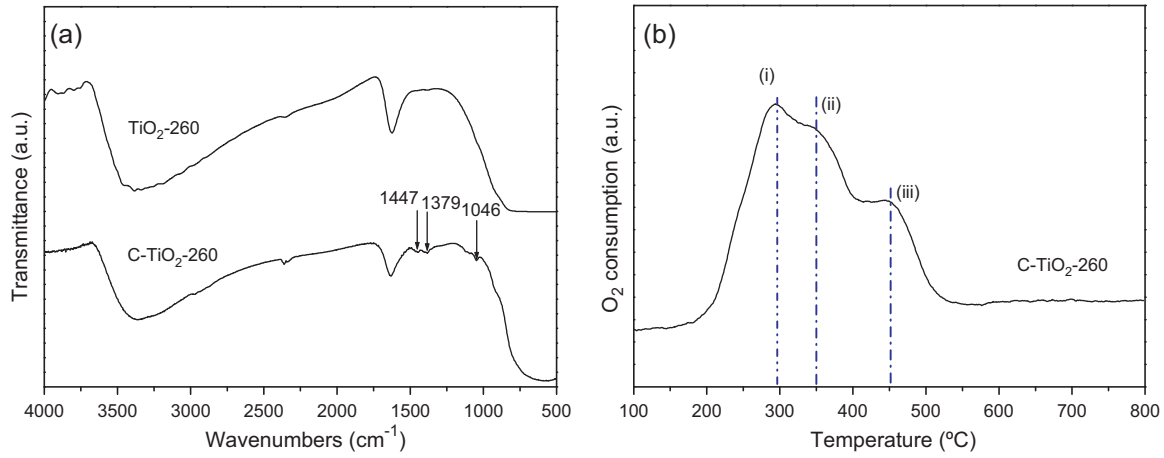

Fig. 4. FT-IR spectrum (a) of TiO_2-260 and C-TiO_2-260 and TPO profiles of C-TiO_2-260.

existing both on the surface and in the framework of TiO_2 were removed after being calcined at 500 °C.

UV–visible diffuse reflectance spectroscopy (DRS) was used to characterize the electronic states of the as prepared sample. Fig. 5a represents the UV–visible absorption spectrum of the pure TiO_2 and carbon modified TiO_2 samples. For large energy gap of anatase (3.10 eV), the former has no significant absorbance for visible-light. The sample of C-TiO_2-260 exhibits a broad absorption bands from 200 to 700 nm with respect to the pure TiO_2, indicating the effective photo-absorption property for this carbon modified TiO_2 photocatalyst system. To the case of a crystalline semiconductor, it was shown that the optical absorption near the band edge follows the equation $\alpha h\nu = A(h\nu - E_g)^n$ [35], where α, ν, E_g, and A are the absorption coefficient, the light frequency, the band gap, and a constant, respectively. Among them, n decides the characteristics of the transition in a semiconductor. Based on the equation, the value of n for TiO_2-based semiconductor is 1 from the data in Fig. 5b. The band gap energy of the as-prepared samples is estimated from the $(ah\upsilon)^{1/2}$ vs. photon energy plots to be 3.10 and 2.04 eV for TiO_2-260 and C-TiO_2-260, respectively. The color of C-TiO_2-260 sample was yellowish, consistent with their photo-absorption spectrum. The chemical reactivity of C-TiO_2-260 was investigated via evaluating the photocurrent generation. As shown in Fig. 5c, the sample of C-TiO_2-260 can generate significant photocurrents under

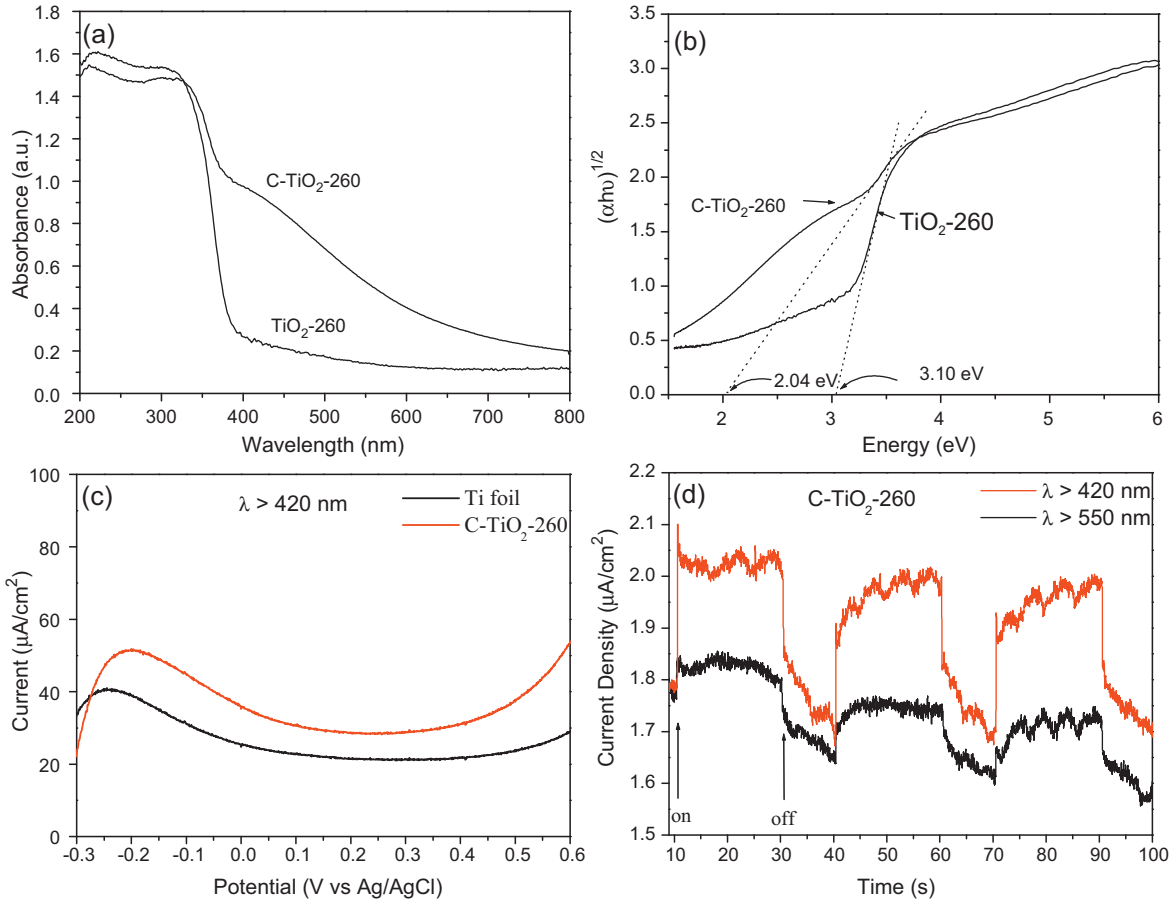

Fig. 5. (a) UV–visible absorption spectra, (b) determination of indirect inter-band transition energies of TiO_2-260 and C-TiO_2-260 samples, (c) photocurrent of titanium foil/C-TiO_2-260 as a function of potential under visible light (λ > 420 nm), and (d) transient photocurrent responses of titanium foil/C-TiO_2-260 biased at 0.5 V under light with a wavelength larger than 420, and 550 nm, respectively.

visible-light irradiation (λ > 420 nm). The photocurrent decreases when increasing the incident-light wavelength, but there was still a noticeable photocurrent found at λ = 550 nm (Fig. 5d). Such excellent photo-electrochemical activity at even longer wavelengths will make such carbon modified TiO_2 an excellent candidate photocatalyst for degrading organic pollutants under visible light irradiation.

3.2. Photocatalytic activity

To evaluate the photocatalytic performance of these C-modified TiO_2 samples, the photo-oxidation of aqueous phenol under visible light irradiation (>420 nm) was used as a photoreaction probe. Fig. 6a shows the relative of phenol removal rate against irradiation time in the presence of photocatalysts under visible-light irradiation. The pure TiO_2 sample (TiO_2-260) shows nearly no activity for degrading phenol. Upon modifying carbon, the phenol removal rate over the C-TiO_2-260 sample reaches about 60% after 2 h irradiation. It shows that the as-prepared carbon-modified TiO_2 samples own an excellent photocatalytic activity for degrading phenol under visible light irradiation.

It should be pointed out that the photocatalytic performance of the as-prepared C-TiO_2 samples was determined by the temperature of the ethanol supercritical condition. Decreasing the temperature to 250 °C resulted in an extreme low removal rate of phenol (about 10%). A removal rate of 39% was obtained when the temperature was increased to 270 °C.

For a clear quantitative comparison, we use the Langmuir–Hinshelwood model (L–H) to describe the rates of the photocatalytic destruction of phenol. The photocatalytic removal rate of phenol was recognized to follow mass-transfer-controlled first-order-kinetics approximately as a result of low concentration target pollutants, as evidenced by the linear plot of $\ln(C_0/C)$ vs. photocatalytic reaction time t (Fig. 6b). The rate constants of the as-obtained samples (TiO_2-260, C-TiO_2-250, 260, and 270) are 0.02041, 0.05491, 0.45182, and 0.24356 min^{-1}, respectively, as shown in Table 1.

It is surprising that the photocatalytic activity of C-TiO_2-250 sample is very poor compared to that of the C-TiO_2-260 sample, though the band gap of the former is about 0.85 eV, much lower than that of the latter, and the other physicochemical parameters of the two samples are nearly same to each other. Such great decrease of activity may be attributed to the excess carbon existing on the surface of TiO_2, which inhibited the transfer of the photo-generated electrons from the sensitizer layer (the out carbon layer) to the surface of TiO_2. As shown in Fig. 7, the color of the C-TiO_2-250 sample is deep gray, and the EDX results of this sample shows that the carbon content is about 15.4 wt.%, much higher than those of the samples synthesized at higher temperature. Increasing the temperature to 270 °C produced a 33% decrease of the activity compared to that (60%) of the C-TiO_2-260 sample. The loss of the activity may be related to its lower surface area (119 m^2/g), broader band gap (2.32 eV) and low carbon content (8.5 wt.%).

In order to identify the activity contribution from the various carbon modification modals, the as-obtained sample (C-TiO_2-260) via supercritical treatment was further calcined at different temperatures (300, 400, and 500 °C) for gradually removing the carbon on the surface and in the lattice of TiO_2 based on the TPO results,

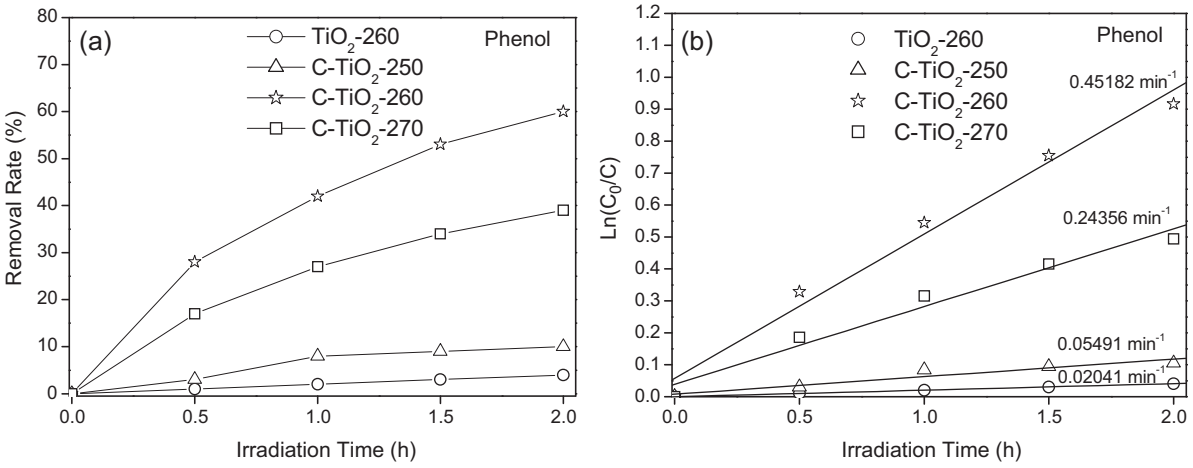

Fig. 6. (a) Plots of the removal rate of phenol vs. irradiation time in the presence of TiO_2-260 (○) and carbon modified TiO_2 synthesized at different supercritical temperature: 250 °C (△), 260 °C (☆) and 270 °C (□) under visible-light irradiation. (b) Dependence of $\ln(C_0/C)$ on irradiation time.

Table 1
Physicochemical properties and activity of the as prepared C-TiO_2 samples.

Samples	S_{BET} (m^2/g)[a]	Pore volume (cm^3/g)[b]	Pore size (nm)[c]	Crystal size (nm)[d]	Band gap (eV)	Removal rate (%)	Rate constant (min^{-1})
TiO_2-260	138	0.19	2.5	11.0	3.10	4	0.02041
C-TiO_2-250	162	0.14	1.8	6.0	0.85	10	0.05491
C-TiO_2-260	160	0.15	1.8	6.1	2.04	60	0.45182
C-TiO_2-270	119	0.15	1.8	7.9	2.32	39	0.24356
C-TiO_2-260-300	144	0.16	1.8	10.2	2.70	65	0.52637
C-TiO_2-260-400	121	0.14	1.9	12.0	2.86	17	0.09065
C-TiO_2-260-500	59	0.09	1.8	12.9	2.98	2	0.00746

[a] BET surface area is calculated from the linear part of the BET plot ($p/p_0 = 0.1–0.2$).
[b] The total pore volumes are estimated from the adsorbed amount at a relative pressure of $p/p_0 = 0.99$.
[c] The pore-size distributions (PSD) are derived from the adsorption branches of the isotherms by using the Barrett–Joyner–Halenda (BJH) method.
[d] $D = K\lambda/(\beta \cos\theta)$, where D is the crystal size, K is the wavelength of the X-ray radiation (0.1541 nm) and usually taken as 0.89, β is the peak widths at half-maximum height of the sample.

and the photocatalytic performances of the calcined samples were also investigated by using the oxidation of phenol as probe reaction. As shown in Fig. 8a, it is obvious that C-TiO_2-260-300 sample possesses the highest activity (65% for removal rate and 0.52637 min^{-1} for rate constant) for degrading phenol, even higher than that (60%) of the C-TiO_2-260 sample, though both the carbon content and the surface area of the former was decreased slightly and band gap was broadened to about 2.70 eV. Such slight increase

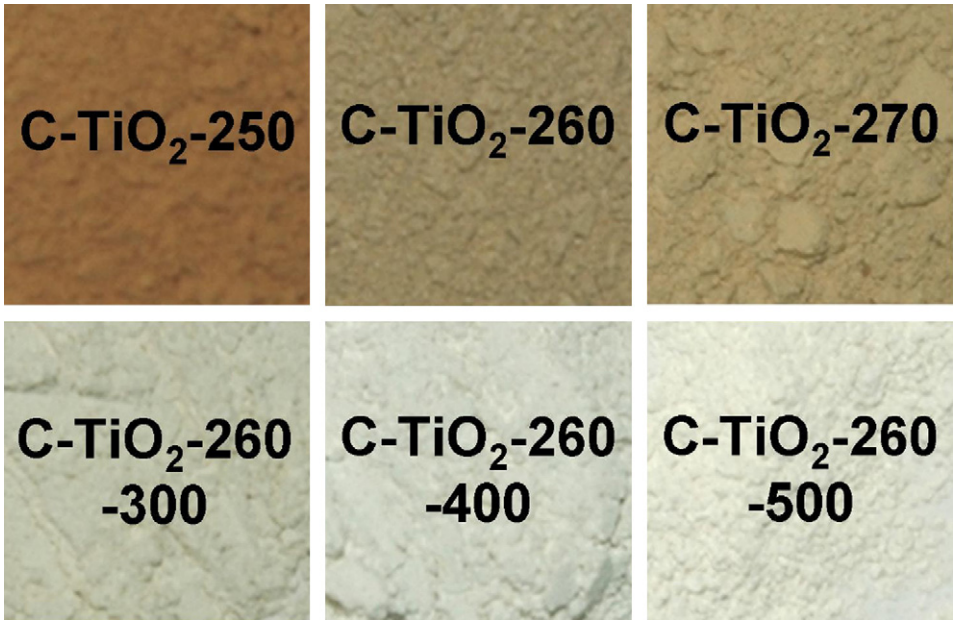

Fig. 7. The color of the as prepared carbon modified TiO_2 samples.

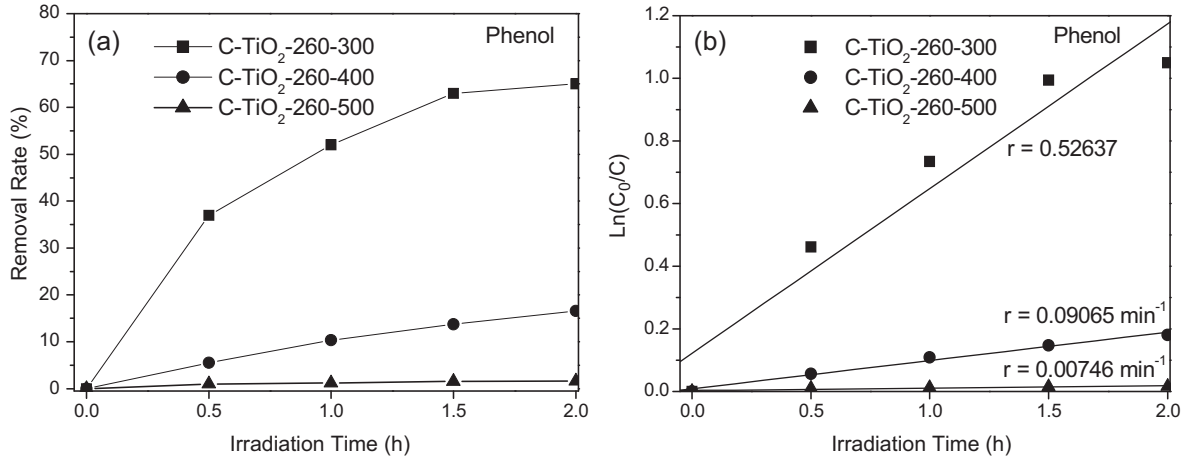

Fig. 8. (a) Plots of the removal rate of phenol vs. irradiation time in the presence of C-TiO_2-260 sample calcined at different temperature: 300 °C (■), 400 °C (●) and 500 °C (▲) under visible-light irradiation. (b) Dependence of ln(C_0/C) on irradiation time.

of the photocatalytic activity could be ascribed to the increased anatase crystallinity. Table 1 shows that the crystal size of C-TiO_2-260-300 is about 10.2 nm, larger than that (6.1 nm) of C-TiO_2-260. As known, a good anatase crystallinity is favorable for enhancing the photocatalytic activity of TiO_2 [26]. When the calcination temperature was raised to 400 °C, nearly all the hybridized carbon grafted onto the surface of TiO_2 was removed based on TPO results and the band gap was increased to about 2.86 eV. It was found that the phenol removal rate of the C-TiO_2-260-400 sample decrease dramatically to about 15% with a low rate constant of about 0.09065 min^{-1}. Further increasing the calcination temperature to 500 °C resulted in nearly no photocatalytic activity for the C-TiO_2-260-500 sample because of the complete removal of carbon and the large band gap of 2.98 eV. These results indicate that the activity contribution from the carbon sensitizing modal is about three folds of that coming from the promotion effect of carbon doped in the TiO_2 lattice. Such synergic effect of the lower band gap induced by the carbon doped into the TiO_2 crystal lattice and photosensitizing resulting from the hybridized carbon grafted onto the TiO_2 surface plays a significant role in the photocatalytic degradation of phenol, as shown in Scheme 1.

The carbon on the surface can effectively enhance the visible light absorption and reduce the reflection of light as a sensitizer, supported by the PL results. Moreover, the carbon on the surface takes up the electrons, promoting the separation of the electrons and holes. In this situation, the surface bound water molecules can be subsequently converted into hydroxyl radicals (•OH). The •OH-trapping experiment was also performed to justify the evolution of hydroxyl radicals during the photocatalytic reaction under visible light irradiation. As shown in Fig. 9a, the

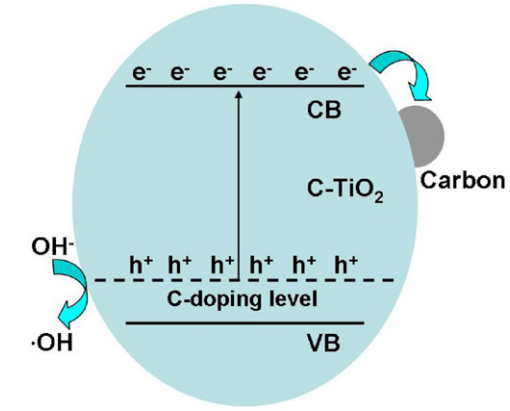

Scheme 1. Proposed photocatalytic mechanism over the C-TiO_2 samples.

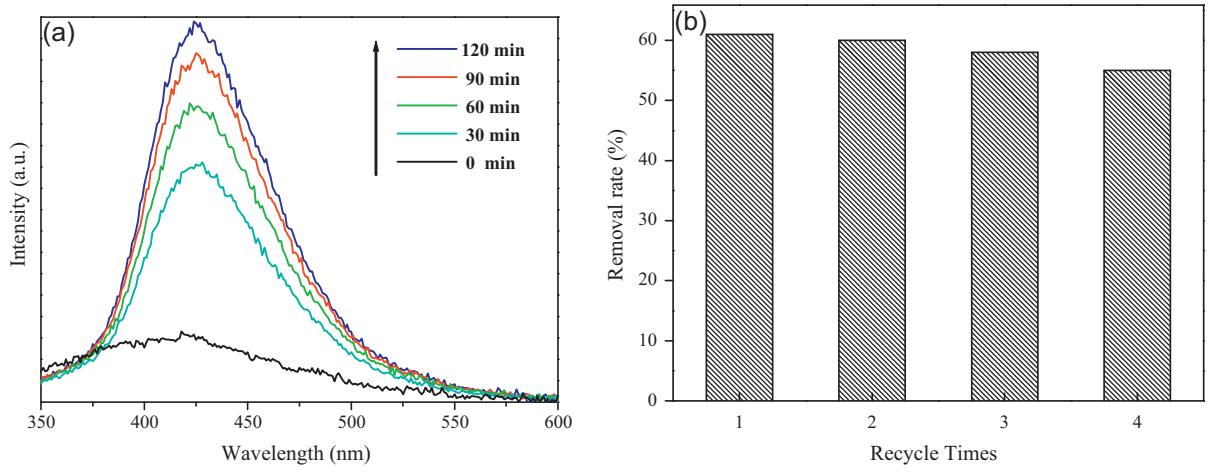

Fig. 9. (a) •OH-trapping photoluminescence spectra of C-TiO_2-260 in 0.05 M terephthalic acid and 0.1 M NaOH solution at different irradiation times (λ > 420 nm; em, 426 nm) and (b) the recyclability of the C-TiO_2-260 sample for degrading phenol.

intensity of the photoluminescence peak at about 426 nm, ascribed to the interaction between terephthalic acid and hydroxyl radicals, increased with extending the visible-light irradiation time. This suggests that hydroxyl radicals do exist in the photocatalytic process.

Though such carbon-induced bimodal synergic effect has allowed the as-obtained samples to exhibit excellent photocatalytic performance for degrading phenol, it is worthy pointing out that the C-TiO_2-260 sample can also possess a perfect recyclability in the degradation of phenol. To test the recyclability, a sample after one trial was washed and dried for the subsequent photoreaction cycles. As shown in Fig. 9b, the removal rate of phenol could be well maintained even after four cycles under visible-light irradiation. Such excellent photocatalytic performance is attributed to its special physicochemical properties, such as mesoporous structure, large BET surface area and high crystallinity of anatase and the bimodal carbon-modification effect induced by the supercritical route.

4. Conclusions

In summary, bimodal carbon-modified mesoporous TiO_2 with high anatase crystallinity and large specific areas was fabricated via an environment friendly and facile ethanol supercritical route. The as-obtained samples exhibit very strong capability for degrading phenol under visible light irradiation ($\lambda > 420$ nm), enhanced visible-light absorption ability and electron–hole separation rate owing to the existing synergic effect originating from the bimodal carbon modification effect, including the doped carbon in TiO_2 lattice and the grafted carbon onto the surface of TiO_2. The resulting findings, reported herein, indicate the promising applications in environmental remediation, which can be further extended to hydrogen evolution via water splitting, solar cells, and etc. The other following explorations for potential applications are in progress.

Acknowledgments

This work was supported by the Program for Professor of Special Appointment (Eastern Scholar) at Shanghai Institutions of Higher Learning, the National Natural Science Foundation of China (21007040, 21047009, 20937003), the Research Fund for the Doctoral Program of Higher Education (20103127120005), the Pujiang Talents Programme and Basic Research Programme of Science and Technology Commission of Shanghai Municipality (11PJ1407500, 10160503200, 11ZR1426300, 07dz22303, 09JC1411400, 10230711600, S30406), and by a Scheme administrated by Shanghai Normal University (SK201104).

References

[1] C.H. Cho, D.K. Kim, D.H. Kim, J. Am. Ceram. Soc. 86 (2003) 1138–1145.
[2] H. Noguchi, A. Nakajima, T. Watanabe, K. Hashimoto, Environ. Sci. Technol. 37 (2003) 153–157.
[3] P.S.S Kumar, R. Sivakumar, S. Anandan, J. Madhavan, P. Maruthamuthu, M. Ashokkumar, Water Res. 42 (2008) 4878–4884.
[4] C.F. Chi, Y.L. Lee, H.S. Weng, Nanotechnology 19 (2008) 125704–125708.
[5] J.C.S. Wu, T.H. Wu, T.C. Chu, H.J. Huang, D.P. Tsai, Top. Catal. 47 (2008) 131–136.
[6] R. Nakamura, T. Tanaka, Y. Nakato, J. Phys. Chem. B 108 (2004) 10617–10620.
[7] H. Irie, Y. Watanabe, K. Hashimoto, J. Phys. Chem. B 107 (2003) 5483–5486.
[8] D. Zhao, C. Chen, Y. Wang, W. Ma, J. Zhao, T. Rajh, L. Zang, Environ. Sci. Technol. 42 (2008) 308–314.
[9] R. Asahi, T. Morikawa, T. Ohwaki, K. Aoki, Y. Taga, Science 293 (2001) 269–271.
[10] C. Belver, R. Bellod, S.J. Stewart, F.G. Requejo, Appl. Catal. B: Environ. 65 (2006) 309–314.
[11] Y. Cong, J.L. Zhang, F. Chen, M. Anpo, D.N. He, J. Phys. Chem. C 111 (2007) 10618–10623.
[12] J.C. Yu, G.S. Li, X.C. Wang, X.L. Hu, C.W. Leung, Z.D. Zhang, Chem. Commun. (2006) 2717–2719.
[13] M. Anpo, M. Takeuchi, J. Catal. 216 (2003) 505–516.
[14] X.G. Hou, F.H. Hao, B. Fan, X.N. Gu, X.Y. Wu, A.D. Liu, Nucl. Instrum. Meth. B 243 (2006) 99–102.
[15] W.Y. Choi, A. Termin, M.R. Hoffmann, J. Phys. Chem. 98 (1994) 13669–13679.
[16] S.U.M. Khan, M. Al-Shahry, W.B. Ingler, Science 297 (2002) 2243–2245.
[17] J.H. Xu, W.L. Dai, J.X. Li, Y. Cao, H.X. Li, H.Y. He, K.N. Fan, Catal. Commun. 9 (2008) 146–152.
[18] H.X. Li, X.Y. Zhang, Y.N. Huo, J. Zhu, Environ. Sci. Technol. 41 (2007) 4410–4414.
[19] H. Irie, Y. Watanabe, K. Hashimoto, Chem. Lett. 32 (2003) 772–773.
[20] H.X. Li, G.S. Li, J. Zhu, Y. Wan, J. Mol. Catal. A 226 (2005) 93–100.
[21] V.G. Courtecuisse, J.F. Bocquet, K. Chhor, C. Pommier, J. Supercrit. Fluids 9 (1996) 222–226.
[22] Y.N. Huo, Z.F. Bian, X.Y. Zhang, Y. Jin, J. Zhu, H.X. Li, J. Phys. Chem. C 112 (2008) 6546–6550.
[23] P. Zabek, J. Eberl, H. Kisch, Photochem. Photobiol. Sci. 8 (2009) 264–269.
[24] L. Zhao, X.F. Chen, X.C. Wang, Y.J. Zhang, W. Wei, Y.H. Sun, M. Antonietti, M. Titirici, Adv. Mater. 22 (2010) 3317–3321.
[25] H.J. Yun, H. Lee, J.B. Joo, N.D. Kim, M.Y. Kang, J. Yi, Appl. Catal. B: Environ. 94 (2010) 241–247.
[26] I. Justicia, P. Ordejon, G. Canto, J.L. Mozos, J. Fraxedas, G.A. Battiston, R. Gerbasi, A. Figueras, Adv. Mater. 14 (2002) 1399–1402.
[27] K.S.W. Sing, D.H. Everett, R.A.W. Haul, L. Moscou, R.A. Pierotti, J. Rouquerol, T. Sieminewska, Pure Appl. Chem. 57 (1985) 603–619.
[28] A.T. Bell, Science 299 (2003) 1688–1691.
[29] W.J. Ren, Z.H. Ai, F.L. Jia, L.Z. Zhang, X.X. Fan, Z.G. Zou, Appl. Catal. B: Environ. 69 (2007) 138–144.
[30] J.J. Xu, Y.H. Ao, D.G. Fu, Appl. Surf. Sci. 256 (2009) 884–888.
[31] H. Wang, X. Quan, H.T. Yu, S. Chen, Carbon 46 (2008) 1126–1132.
[32] J.C. Parker, R.W. Siegei, Appl. Phys. Lett. 57 (1990) 943–945.
[33] Y. Huang, W.K. Ho, S.C. Lee, L.Z. Zhang, G.S. Li, J.C. Yu, Langmuir 24 (2008) 3510–3516.
[34] J.B. Yin, X.P. Zhao, J. Colloid Interface Sci. 257 (2003) 228–236.
[35] J.C. Yu, X.C. Wang, X.Z. Fu, Chem. Mater. 16 (2004) 1523–1530.